Magnetorheological Valve for Hybrid Electrohydrostatic Actuation

DAVID T. NOSSE AND MARCELO J. DAPINO*

Department of Mechanical Engineering
The Ohio State University, Suite 255, 650 Ackerman Road
Columbus, OH 43202, USA

ABSTRACT: There is an increasing demand for compact actuators capable of producing large deflections, large forces, and broad frequency bandwidths. Due to their solid state nature, smart materials can enable novel actuator solutions that compete favorably with established technologies based on electric, hydraulic, or pneumatic motors. However, in all existing active materials, large force and broadband responses are obtained at small displacements and methods for transmitting very short transducer element motion to large deformations need to be developed. We present a new hybrid actuator which operates on the principle of rectification of magnetostrictive vibrations by means of magnetorheological (MR) flow control. Experiments and theoretical calculations are aimed at substantiating the feasibility of the hybrid actuator and establishing design criteria for the development of an effective MR valve. The experiments presented here demonstrate the ability of the valve to completely block the flow due to the combined action of a pressure differential and MR fluid activation. For characterization purposes, two variations of the main valve concept are considered, one with moving coils and the other with fixed coils. Actuation measurements conducted on the complete actuator show deflections of 6.5 in. in response to fluid inputs produced with a hydraulic piston in combination with an applied quasistatic voltage of amplitude 5 V. A system-level model is presented which is developed by treating the system as an RLC equivalent electrical circuit with operation across electrical, mechanical, and fluid domains. Attributes and shortcomings of the model are discussed through comparison of model results with experimental data.

Key Words: hybrid actuator, rectification valve, magnetorheological (MR) fluid, magnetostrictive pump, Terfenol-D, magnetorheological fluid valve, electrohydraulic actuation.

INTRODUCTION

TRADITIONAL actuators based on electric, hydraulic, or pneumatic technologies are widely used in components and systems requiring automated displacement, force, rotation, and torque. However, a new class of actuators is needed that can satisfy currently unmet performance demands concerning power density, miniaturization, reliability, and frequency bandwidth. Specific applications which can benefit from new and improved actuator technologies include, among others, compact haptic interfaces, control surfaces for unmanned vehicles, actuator-based active suspension systems for heavy-duty commercial vehicles, adaptive airframes, and robotic locomotion components.

Smart materials can enable new actuators with few moving parts and reliable operation, concurrently with large frequency bandwidth, compact size, and high power density. Some of the smart material transduction technologies being investigated can in certain cases exceed the power density of conventional electromagnetic and hydraulic devices, as is the case for example with nickel titanium alloys. In these alloys, however, large displacements are obtained at the expense of small forces or slow responses. Materials with faster reaction times, such as magnetostrictive or piezoelectric materials, have insufficient energy densities, so use of these materials is typically restricted to low-displacement, high-force applications. Novel methods for converting very short deformation into large motion must therefore be developed.

The objective of this article is to present a new type of electrohydraulic actuator, with emphasis on characterizing and establishing design criteria for its magnetorheological (MR) fluid-based rectification mechanism. The principle for achieving motion amplification in this actuator is based on two effects: (i) rectification of the resonant vibrations produced by a

*Author to whom correspondence should be addressed.
E-mail: dapino.1@osu.edu
Figures 1–18, 20 and 21 appear in color online: http://jim.sagepub.com

1045-389X/07/11 1121–16 $10.00/0 DOI: 10.1177/1045389X06072359
© SAGE Publications 2007
Los Angeles, London, New Delhi and Singapore

magnetostrictive motor by means of magnetorheological flow control, and (ii) hydraulic advantage for conversion of magnetostrain into large forces. The study is focused on two specific aspects of actuator development. The first is the development of a four-port MR fluid valve to magnetically control the flow of MR fluid. Closure of the valve is produced by the combined action of a pressure differential created by a fluid source and the increase in effective viscosity of an MR fluid with applied magnetic fields. Since the rectification must be performed at very high speeds, design and performance criteria for the development of an effective, fast-acting MR valve are discussed. The second component of the study is to prove the feasibility of the proposed hybrid actuator both experimentally and analytically.

The most advanced magnetostrictive material, Terfenol-D, can produce static strains on the order of 0.16% at fields of 150 kA/m and loads of about 14 MPa. One method considered for achieving amplified actuation consists of combining a magnetostrictive pump with a conventional hydraulic cylinder and a set of flow valves. Gerver et al. (1998) developed a pump for space applications which includes a Terfenol-D driver connected to a hydraulic stroke amplifier. The pump produces a flow rate of 30 ml/sec and a pressure of 5 psi, for a total power consumption of 25 W. Bridger et al. (2004) developed a high-pressure unit designed on the basis of resonant motion. This pump produces a pressure of 3000 psi and has a high electromechanical coupling of 60%. Other methods considered for amplifying the small deformations produced by magnetostrictive materials include mechanical amplifiers (Claeyssen and Lhermet, 2002; Lhermet et al., 2004), and inchworm actuators (Kiesewetter, 1998; Teter et al., 1998). However, these methods have intrinsic problems such as wear and backlash.

Piezoelectric stack actuators have been extensively used in hydraulic fluid pumps (Lee et al., 2004; Mauck and Lynch, 2000; Sirohi and Chopra, 2003) as well as inchworm devices (Park et al., 2000) and kinematic linkages (Canfield and Frecker, 2000; Prechtl and Hall, 1999) for the purpose of large linear motion. Although commercially available piezoelectric stack actuators are capable of generating strains of 0.10–0.15% and potentially larger deformations via motion amplification mechanisms, the operating frequency and amplitude of these deformations are limited by dielectric losses and self-heating. Normal low-voltage actuators with mid-sized diameters tend to overheat at frequencies in the range of about 200 Hz at full stroke operation, which severely limits the rate of actuation. Piezohydraulic actuators are thus attractive so long as the temperature of the stack can be controlled. Sirohi and Chopra (2003) were able to increase the frequency of steady state operation of a piezoelectric pump to 1000 Hz by using a thermally conducting silicone heat sink, but they accomplished so at the expense of overall system efficiency. This device achieved a blocking force of 35 lbs and a no-load velocity of 1.2 in./sec. A later study by Sirohi et al. (2005) was aimed at characterizing the dynamics of piezohydraulic actuators by considering the effects of fluid compressibility, inertia, and viscosity.

Electrohydraulic actuators that use active valves for rectification have also been considered. An actuator concept proposed by Lhermet et al. (2004) employs a magnetostrictive pump and a set of unidirectional valves, which consist of a magnetostrictive or piezoelectric element coupled to a compliant structure that acts as a motion amplifier. A prototype device achieves pressures of 40 bar, flow rates of 0.4 l/min, and hydraulic power of 27 W. However, this prototype can only operate at a frequency of 10 Hz, significantly lower than the target frequency of 400 Hz. A much faster response of 15 kHz was achieved by a piezoelectric-hydraulic pump with unimorph disc valves proposed by Lee et al. (2004). A prototype pump has been shown to achieve a flow rate of 3.4 cc/sec, a pump-specific power density of 12 W/kg, and a stall pressure of 8.3 MPa.

Magnetorheological fluids undergo an apparent increase in viscosity within milliseconds of being exposed to a magnetic field (Jolly et al., 1998). This principle has been used in semi-active dampers for implementation in a variety of applications including civil infrastructures (Jung et al., 2004) automotive and industrial clutches (Cobanoglu et al., 2003), aeronautical systems (Choi and Wereley, 2004), and biomedical manipulators (Neelakantan et al., 2002). A less common alternative is the use of MR fluids in active actuators that combine a pump, MR fluid valves and a hydraulic cylinder. The pump design presents challenges concerning wear of the pump head components due to abrasion by the MR fluid particles. In terms of MR valve design, one configuration by Yoo and Wereley (Yoo et al., 2003, 2005; Yoo and Wereley, 2004) consists of a set of four MR valves configured as a Wheatstone bridge hydraulic circuit. Each valve includes an annular path for MR fluid; the pressure differential across the gap is adjusted by applying a magnetic field with a coil embedded in the valve. Important advantages of this valve system over mechanical valves include the lack of moving parts and a fast frequency response. One disadvantage is that full closure of the valve is never possible due to the finite yield stress of MR fluid, which reaches 45 kPa when activated by a magnetic field of intensity 250 kA/m, thus causing a significant loss in system efficiency.

PRINCIPLE OF OPERATION OF THE HYBRID ACTUATOR

The main components of the hybrid magnetostrictive–magnetorheological actuator are shown in

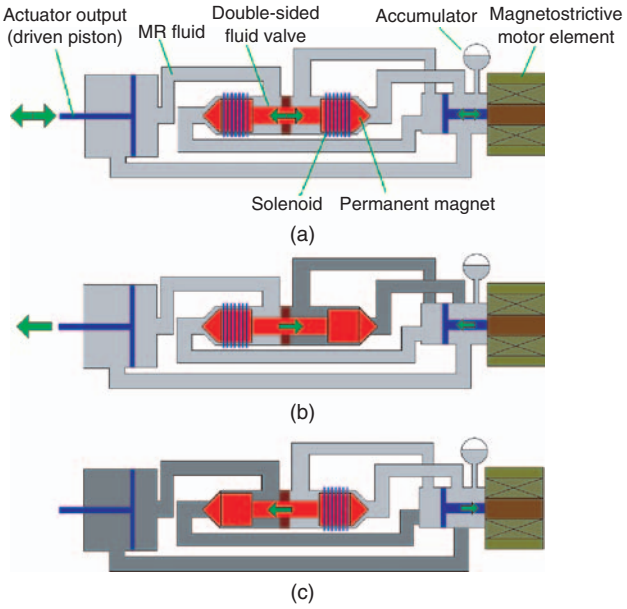

Figure 1. *(a) Hybrid MR fluid-magnetostrictive actuator; (b) the drive piston connected to the Terfenol-D pump pushes the fluid through the left valve half and subsequently pushes the driven piston on the load end (left coil active), while the right valve half remains closed; (c) the drive piston retracts while the MR fluid recirculates through the right valve half (right coil active). The driven piston stays fixed until step (b) starts again and the sequence is repeated. Permanent magnets inside the conical heads provide a bias magnetization on the MR fluid.*

Figure 1(a)–(c). The system consists of a four-port MR fluid valve, MR fluid, Terfenol-D motor, drive piston, and driven piston. To achieve rectification of the resonant vibrations produced by the Terfenol-D motor, and thus large deflections, the actuator operates by cyclic repetition of two stages, actuator extension and fluid refill. At each stage, the MR fluid valve completely closes one half of the fluid circuit and permits free flow through the other.

Flow generated by the Terfenol-D pump and drive piston is routed through two flow paths which are connected in parallel, i.e., they share a common pressure differential. Each fluid route includes one half of the MR fluid valve, and one path includes a driven piston for conversion of flow into linear actuation. The MR fluid valve has two conical heads, each fitted with a permanent magnet. A solenoid wrapped around each conical head is used to cancel the field produced by the permanent magnet. With no current applied to the solenoid, there is no magnetic field cancellation and the MR fluid in the vicinity of the conical head increases in effective viscosity. When a suitable current is applied, the fields from the solenoid and permanent magnet cancel each other out and the MR fluid decreases in viscosity, thus permitting flow through the valve. This design creates a normally closed mechanism that locks the actuator in place in the event of power failure.

The actuator extension stage commences with the leftmost solenoid turned on and the rightmost turned off, as shown in Figure 1(b). This effectively thickens the MR fluid in the right path, producing a fluid path of least resistance through the left valve half. The flow produced by the Terfenol-D pump produces a pressure differential that fully closes the right valve half with the assistance of the MR fluid, which when energized by magnetic fields behaves as an o-ring around the conical head. Once the right valve half has closed, the flow extends the driven piston for positive actuation. To increase the output force, a hydraulic advantage is created by implementing a driven piston diameter that is larger than the drive piston.

The fluid refill stage immediately follows as the Terfenol-D element and drive piston begin to retract, as shown in Figure 1(c). To refill the fluid cavity without also retracting the actuator output, the left solenoid is turned off and the right turned on. This changes the fluid path of least resistance and creates the pressure differential necessary to begin closing of the left valve half. With the left half closed, the actuator output is temporarily locked, and the free flow path through the right valve half refills the cavity. Steps (b) and (c) are subsequently repeated at high speed to further extend the driven piston and thus achieve quasi-continuous motion of the load attached to the actuator. Figure 2 shows the ideal timing diagram for the Terfenol-D pump and MR fluid valve.

It is emphasized that complete closure of each conical head is possible only under the combined action of the pressure differential created by the pump and the MR fluid acting as a seal around the conical head when energized. Use of a fluid without magnetorheological properties therefore cannot produce full closure of the valve. Evidence supporting this characteristic of the system is presented in the section 'MR valve feasibility measurements'.

EXPERIMENTS

A prototype four-port, two-sided MR valve as illustrated in Figure 3 was constructed and tested for purposes of proof-of-concept validation, model verification and system parameter identification. The valve consists of two conical heads, each embedded with two solenoids and no permanent magnets. In this valve, power must be applied to the solenoids for it to close. The result is a normally open MR valve which is easier to implement than its normally closed counterpart while providing greater flexibility to adjust the applied magnetic field. To further improve adjustability and observability, the fluid valve has a symmetric architecture which consists of two identical valve halves externally coupled together. This configuration has several advantages as it allows to adjust the total length of valve travel from fully closed to fully open,

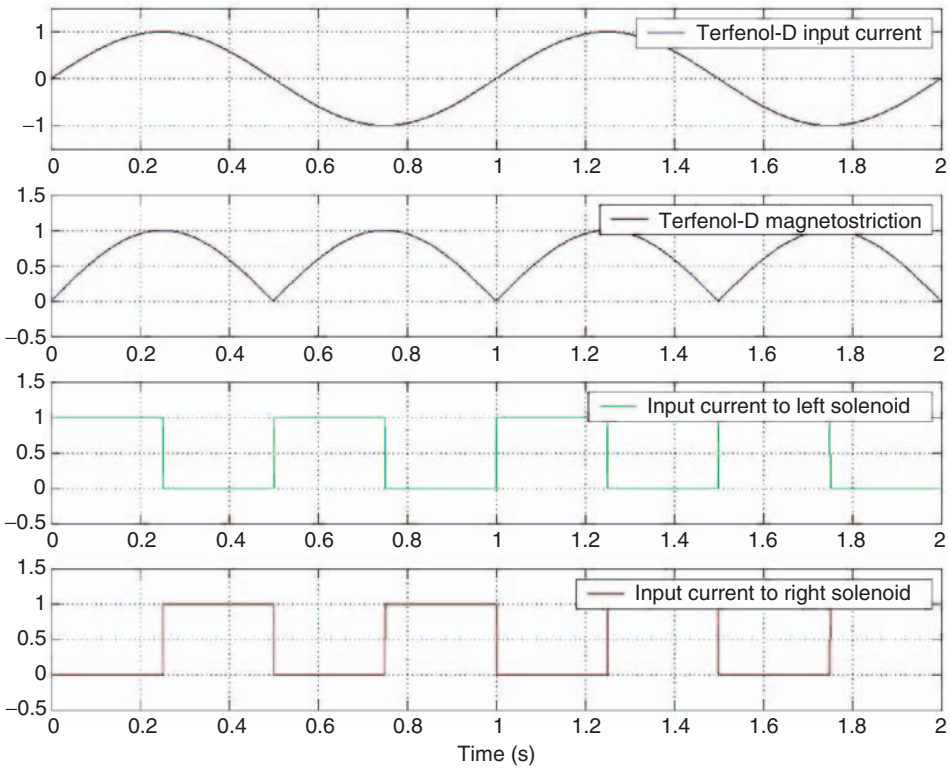

Figure 2. *Timing diagram for the Terfenol-D pump and MR fluid valve.*

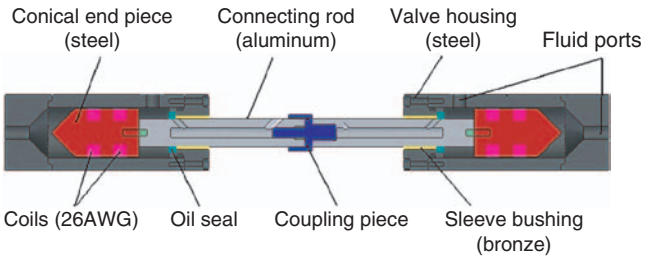

Figure 3. *Cutaway solid model of the MR fluid valve. The grooves in the conical valve ends are fitted with coils rather than permanent magnets, for enhanced flexibility during system development.*

use simple displacement sensors, control the initial position of the valve shaft, visually inspect the motion of the valve, and fix the valve shaft at an arbitrary location for operation as a fixed-shaft valve.

The simultaneous requirement of high flow rate and high pressure needed to operate this oversized valve complicates the development of a matching Terfenol-D pump. In this study, to circumvent this limitation during valve development, the fluid inputs are generated by a double-ended hydraulic piston driven by a hand pump or a universal compression–tension machine. The three major components, fluid valve, input piston, and output piston, are connected by steel lines to form a closed MR fluid network. Instruments directly connected to the system include a laser position sensor to record valve location, a precision string potentiometer to record output actuation, two diaphragm pressure sensors, and a load cell and linear variable differential transducer (LVDT) to record forces and displacements produced by the compression–tension machine. A LabVIEW virtual instrument provides both data acquisition capabilities and automated control of the MR fluid valve's solenoids.

MR Valve Feasibility Measurements

It was indicated in the section 'Principles of operation of the hybrid actuator' that the MR fluid valve operates under the combined action of a pressure differential and an increase or decrease in the effective viscosity of an MR fluid. The ability of the valve to shut completely and hold pressure without leakage at relatively high pressures of 600–800 psi was established by Burton et al. (2004). We are now interested in investigating the ability of the MR valve to control the flow at lower pressure differentials, thereby enabling the use of a smaller pump to drive the hybrid actuator. The experimental setup, shown in Figure 4(a) and (b), consists of a hydraulic pump, fluid network, and MR fluid valve.

In Figures 5–7, the ability of the valve to operate with both a pressure differential and voltage-induced viscosity change is shown. The valve position data has been normalized by translating it on the time axis and scaling

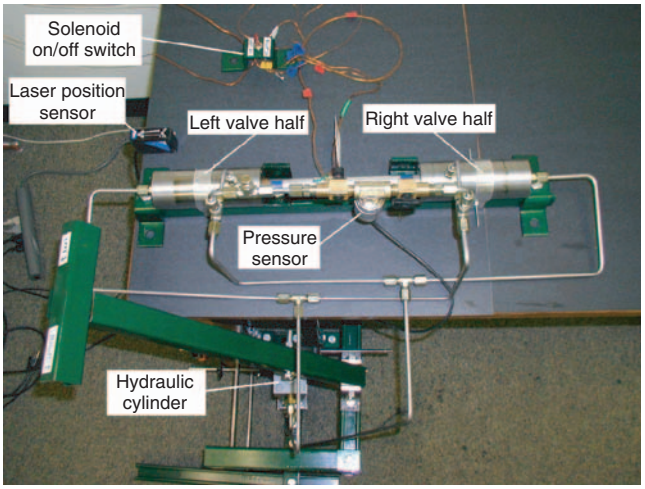

(a)

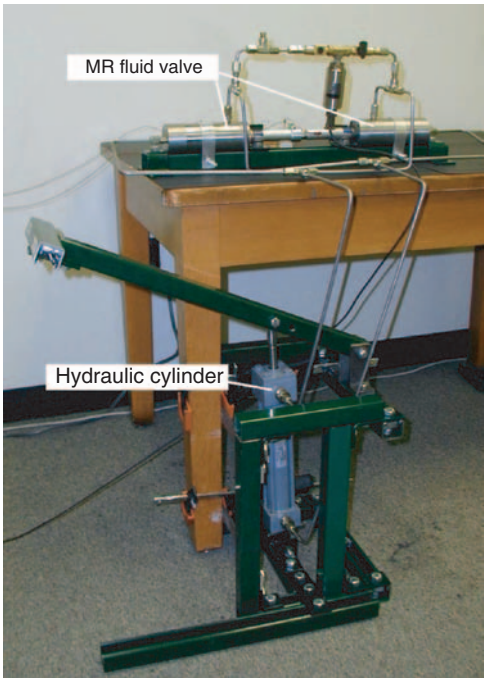

(b)

Figure 4. *(a), (b) Experimental setup used for testing of the four-port MR fluid valve.*

it by the (min/max) ratio. Noise peaks in the data cause the nominal 0.0 (left closed) and 1.0 (right closed) points to be shifted slightly. In Figure 5, a dc voltage of 20 V was applied to the right solenoid while the manual hydraulic cylinder was extended up. Immediately after the right valve half was closed, an identical voltage was applied to the left solenoid, followed by a manual retraction of the hydraulic cylinder. This cycle was run for a duration of over 12 s at ~0.7 Hz, resulting in an average flow rate of 12 $in.^3/s$. Figure 6 shows the measured pressure from the left valve half from a similar run. It is seen that the fluid valve cycles between fully closed left to fully closed right with the appropriate combination of pressure differential and viscosity change. The variations in the pressure recordings from the left and right sides are attributed to the volume change caused by the single-ended hydraulic cylinder's connecting rod. As the piston is extended, the volume of the rod is removed from the upper piston half, but not the lower piston half. Dissimilar pressure differentials across the system are produced for each hydraulic pump direction.

Figure 7 presents the measurements obtained by conducting the above test with an input of 5 V rather than 20 V. The MR fluid valve was able to cycle between fully closed and fully open despite the lower input voltage. Furthermore, it is observed that less force on the hydraulic cylinder was required to produce the same valve motion. This implies that for this system, low voltages close to 5 V could offer efficiency and performance advantages over larger voltages. The lower force requirement at 5 V excitation is attributed to lower magnetic inductance creating a lower apparent fluid viscosity and damping force. As shown in Figure 8, the valve is operated with only a pressure differential (zero solenoid voltage), with the manual hydraulic cylinder pumped hard enough to create over 100 psi of peak line pressure. The MR fluid valve was biased to both closed positions in subsequent tests. While very small motions are observed, the pressure differential alone is not sufficient to operate the MR valve; the MR behavior of an MR fluid is indeed required for this valve to open and close in a controlled manner.

Actuation Results

We are now interested in determining the ability of the MR valve to operate while connected to an output piston. The fluid input is in this case generated by a double-ended hydraulic piston – which helps to address the asymmetries in the fluid network discussed in the previous section – connected to a universal compression–tension machine (Figure 9). A schematic illustrating the system and reference directions is shown in Figure 10(a)–(c).

A net actuation of 6.5 in. was achieved at a rate of 0.325 in./s from a 1.0 in., 0.5 Hz sine wave drive piston input and 5 V square wave applied during negative (F1) input piston loading to the left valve half. The mechanical and electrical inputs are plotted in Figure 11(a), whereas the pressure measurements are shown in Figure 11(b). The output actuation motion, shown in Figure 11(d), is a ramped sinusoid. The control strategy outlined in the second section involves applying square waves at a relative phase of 180° between each solenoid. It was determined that in this system, however, application of voltage to the right solenoid, which is placed in series with the output piston, has no effect on the ability of the actuator to produce output motion. This is attributed to the

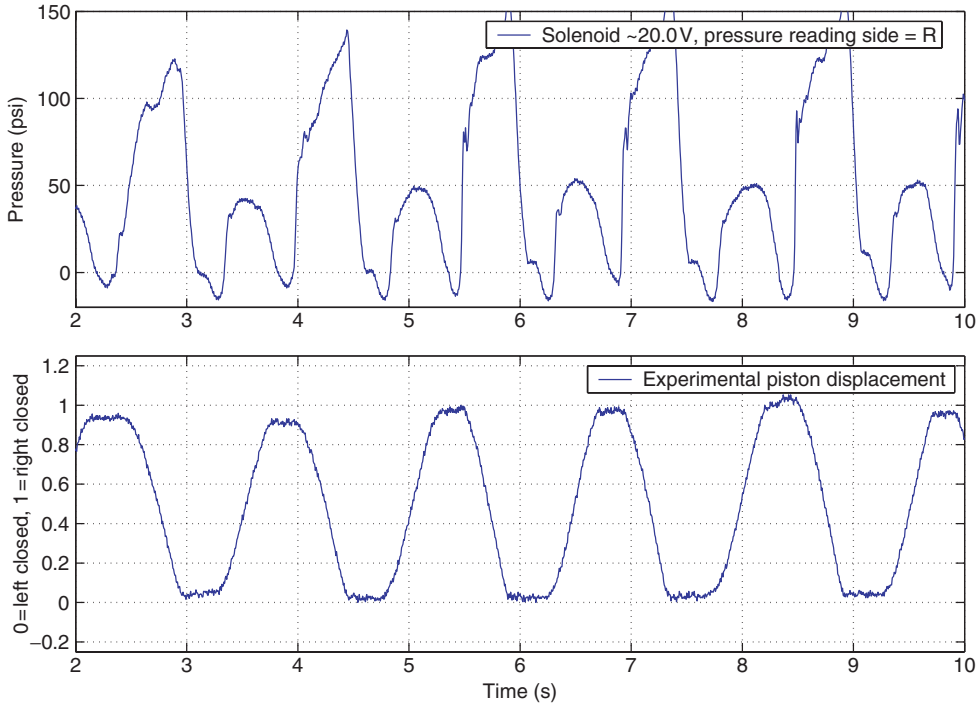

Figure 5. *Tests for right valve half, 20 V input.*

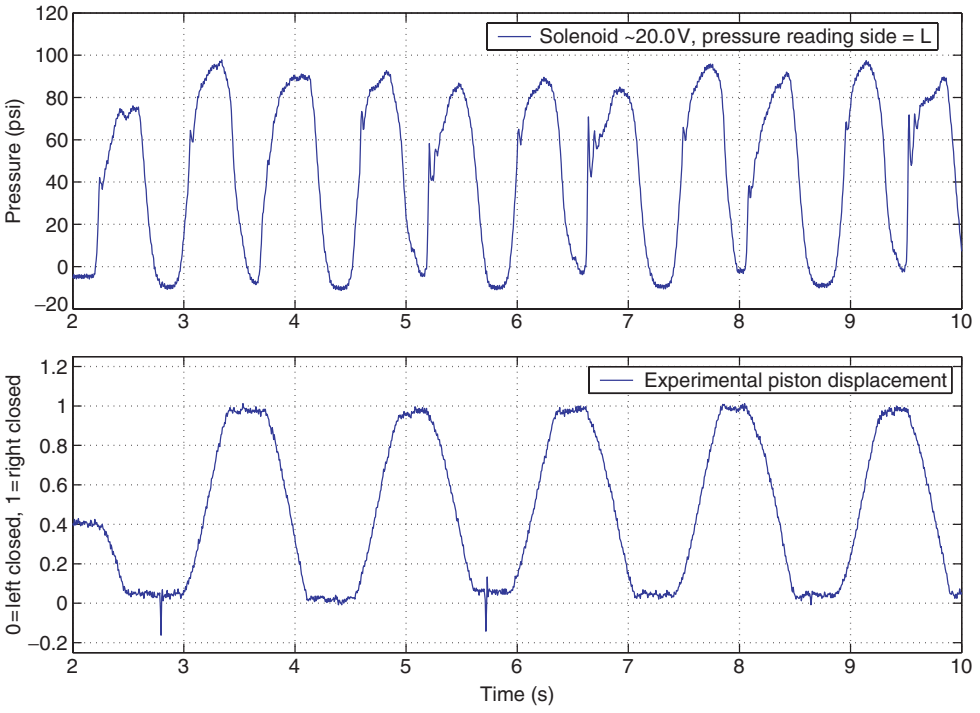

Figure 6. *Tests for left valve half, 20 V input.*

unequal fluid resistance of the two fluid paths, which implies the asymmetries were not completely addressed by including a double-ended drive cylinder. Due to the asymmetric fluid network configuration imposed by the output piston, the left valve half establishes a path of least resistance regardless of the state of the right valve half. This asymmetry is ultimately responsible for the partial motion reversal (recoil) of the output piston and associated decrease in system efficiency. Notwithstanding, the ability of the system to produce a net positive displacement is established.

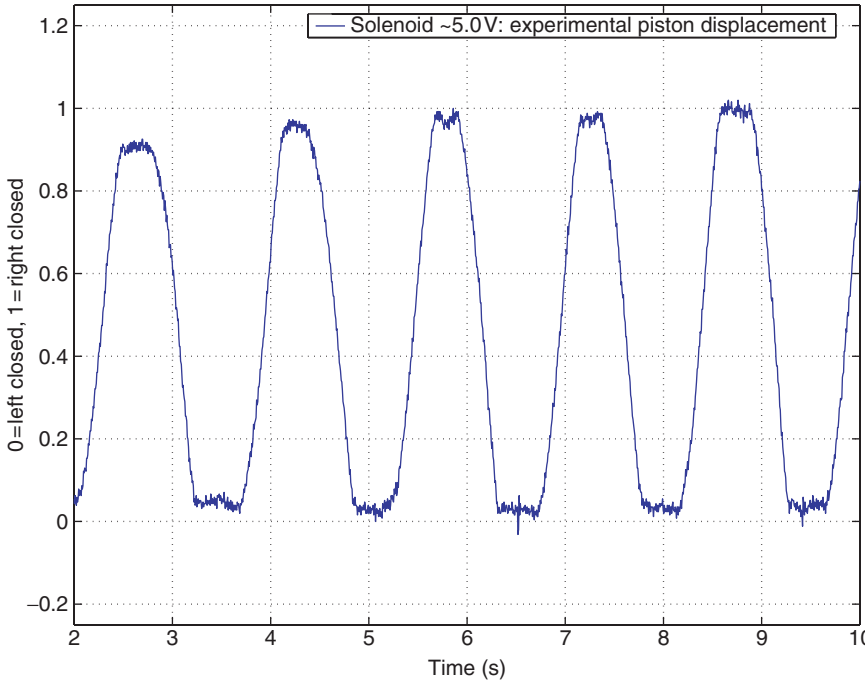

Figure 7. *Tests for left valve half, 5 V input.*

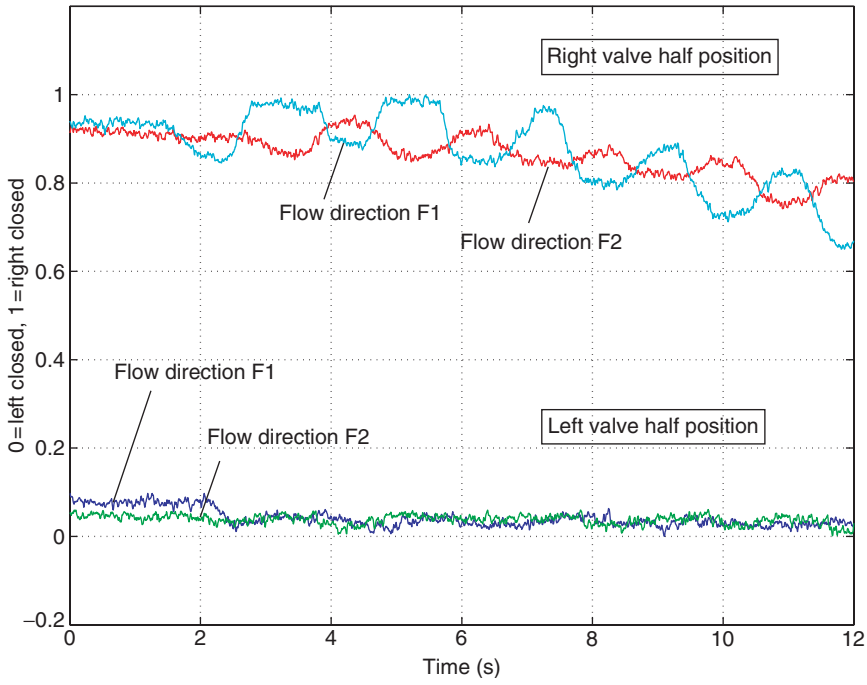

Figure 8. *Zero voltage test.*

Another departure from ideal behavior is that the MR fluid valve does not close completely one half, then completely close the other valve half. Instead, it quickly moves toward the controlled solenoid side (side not in series with output piston) and fluctuates small amounts from completely closed to slightly open. This is attributed to large sliding frictions observed in the valve becoming more dominant due to smaller volume flow rates and asymmetrical flow paths. This behavior is illustrated in Figure 11(c). As in section 'MR valve feasibility measurements', large volume flow rates and symmetrical flow paths dominated the sliding friction.

The results point to the following design criteria which need to be satisfied in order to address these deviations

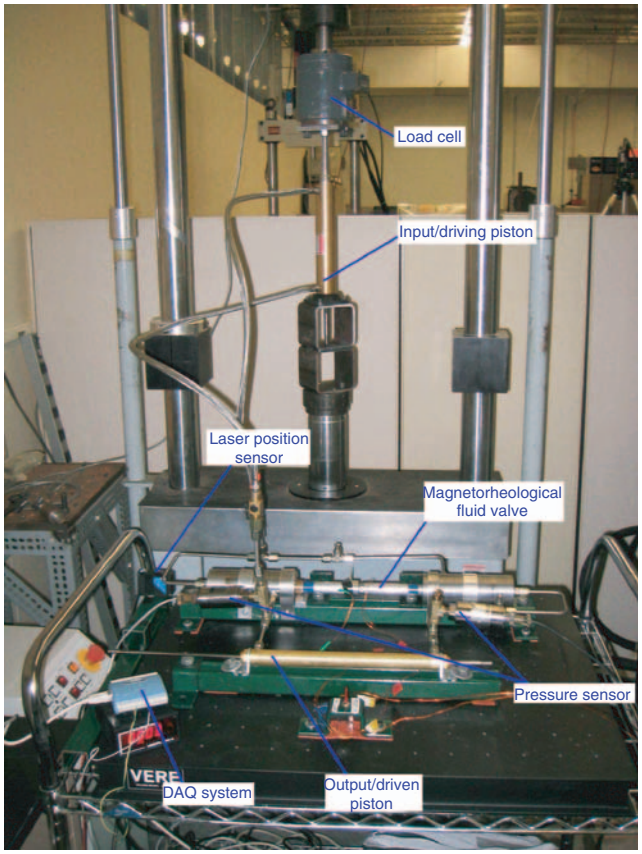

Figure 9. *Experimental setup used for development and testing of the MR fluid valve and hybrid actuator.*

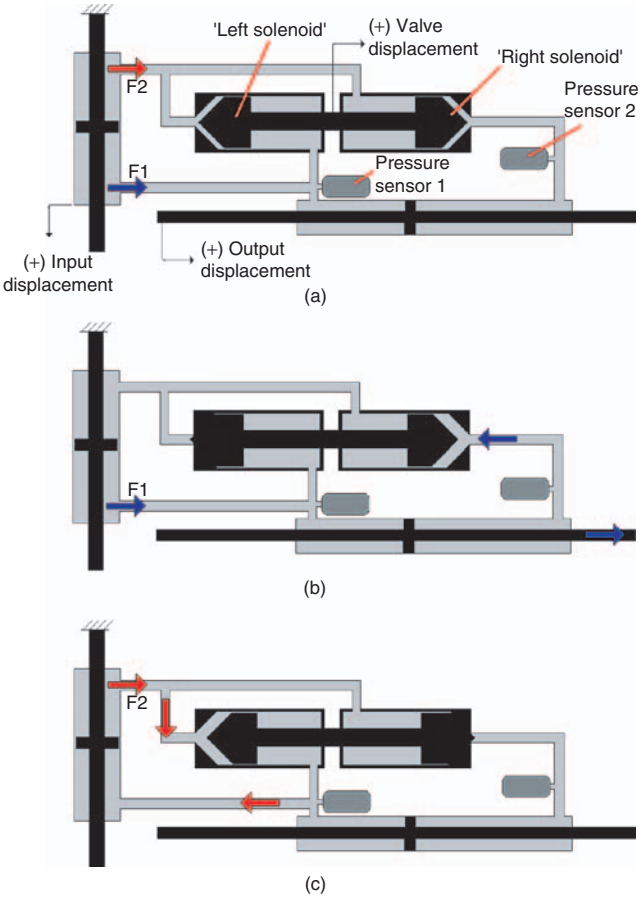

Figure 10. *System used for characterization of the MR valve, consisting of a drive piston connected to a tension–compression machine, MR valve and output cylinder: (a) reference directions; (b) actuation step; and (c) refill step needed to complete one actuation cycle. A positive input displacement produces flow F2 and negative input displacement produces flow F1.*

from ideal behavior: (i) the off-state resistance of the valve and static friction of the output piston must be reduced as much as possible in order to not only minimize power losses but contribute to an overall balance in the fluid resistance paths; (ii) the on-state resistance of each valve half must be as large as possible to ensure controlled closure of the valve; and (iii) the length and compliance of the fluid lines must be as small as possible.

Fluid Resistance Measurements

We now investigate the factors that affect criteria (i) and (ii) outlined in the previous section. Two designs are considered, one with coils placed in the conical head and the other with coils placed in the valve housing. The latter design approach is shown to provide improved performance in a reduced package. The parameters that are varied in this study are the solenoid voltage, axial gap size, annular gap size, and flow direction. The conical head angle is 90° as shown in Figure 12.

EXISTING VALVE (COILS IN SHAFT)

The experimental setup employed for the resistance measurements is shown in Figure 13(a). The valve shaft is rigidly held to maintain a constant axial gap throughout the duration of each run. This gap can be adjusted and then locked to isolate the effect of valve shaft location. Measured quantities include the position of the universal compression–tension machine, from where the flow rate Q_v is calculated, and the pressures $P1$ and $P2$ on either end of the valve. The fluid resistance is then calculated by

$$R = \frac{|P2 - P1|}{Q_v}. \tag{1}$$

To remove unwanted dynamic effects from the measurements, a triangular waveform of amplitude 4 in. pk–pk and frequency of 0.25 Hz was selected as the displacement applied by the universal compression–tension machine to the input piston (Figure 14(a) and (b)). This produces constant MR fluid volume flow rates between peaks of 3.25 $in.^3/s$. Although the input flow rate was the same for all resistance runs, the applied force varied considerably as it depends on the resistance of the fluid path.

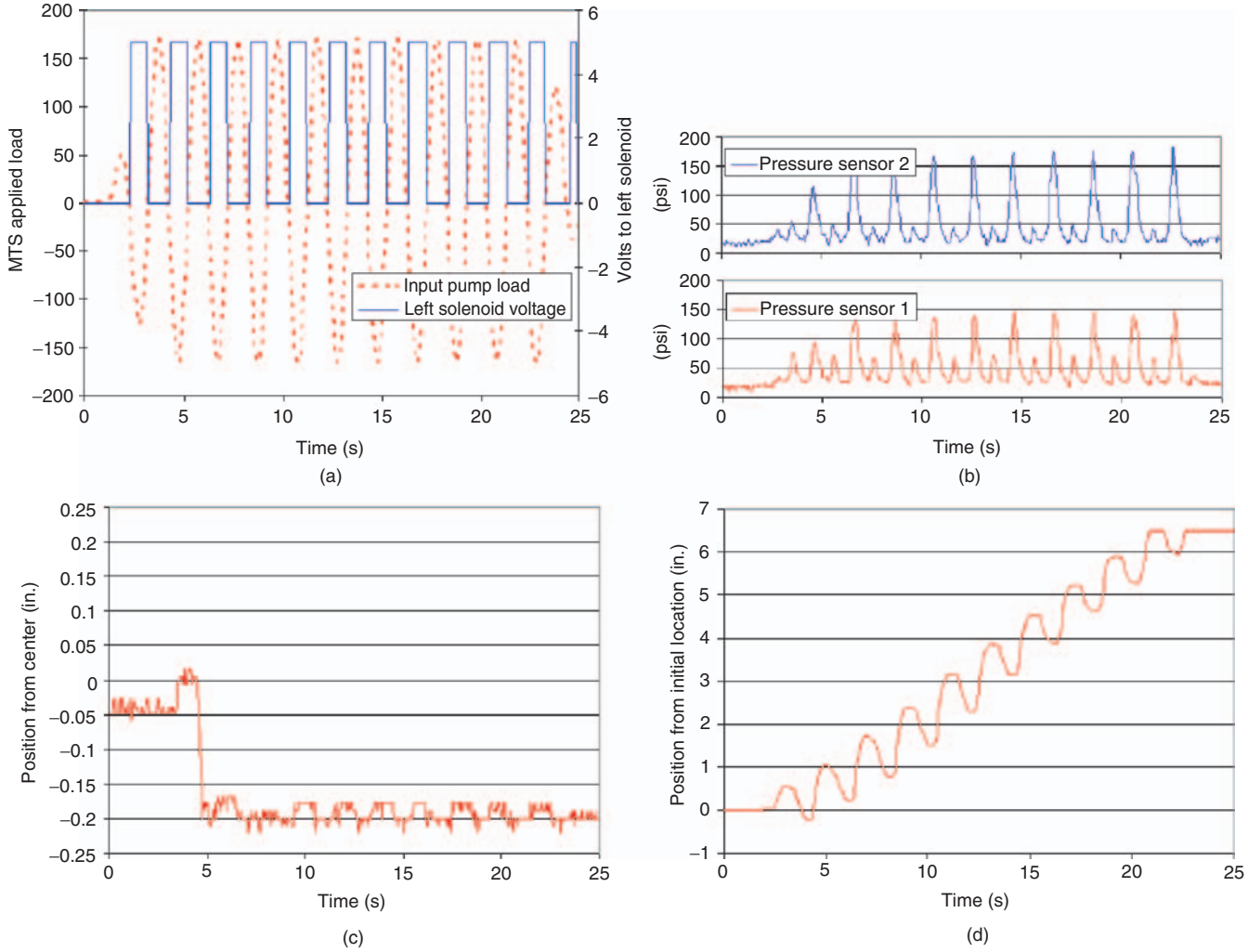

Figure 11. *Actuation results: (a) control strategy for 5 V dc solenoid input and negative (F1) input piston loading; (b) line pressures measured near the cylinder ports as shown in Figure 9; (c) valve shaft location; and (d) output piston position.*

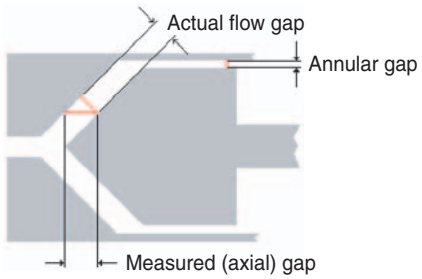

Figure 12. *Illustration of MR fluid valve gap terminology.*

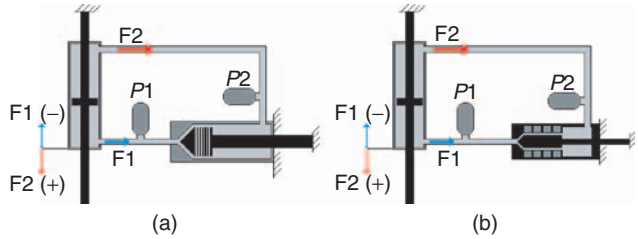

Figure 13. *Illustration of setup used to determine the resistance of an MR valve with solenoids in: (a) shaft and (b) housing. Arrows depict the two flow directions, F1 and F2, based respectively on negative and positive motion of the input cylinder.*

The valve employed in these tests has an annular gap of 0.030 in. In addition, a new valve shaft with smaller conical diameter was constructed to provide an additional annular ring dimension of 0.125 in. when mounted in the existing valve housing.

To illustrate typical resistance measurements, in Figure 15(a) are shown the line pressures for an input of 10 V, axial gap of 0.125 in. and annular gap of 0.030 in. The difference between the line pressures is the pressure drop $|P2 - P1|$ across the valve, shown in Figure 15(b). The flow directions F2 and F1 respectively correspond to positive and negative pressure differentials. The calculated fluid resistance is shown in Figure 15(c).

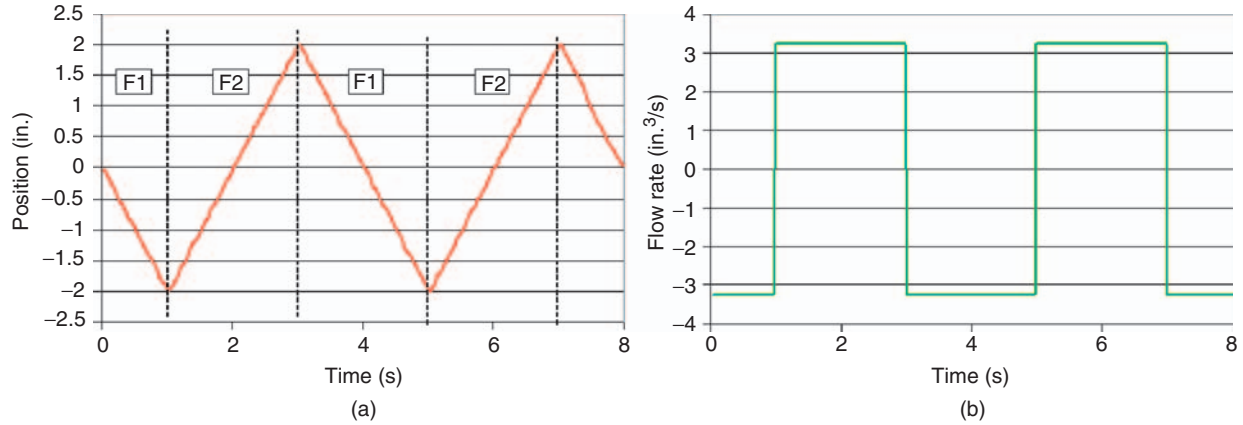

Figure 14. *(a) Input waveform produced by the universal tension–compression machine and (b) calculated input flow rate for resistance testing of MR fluid valve.*

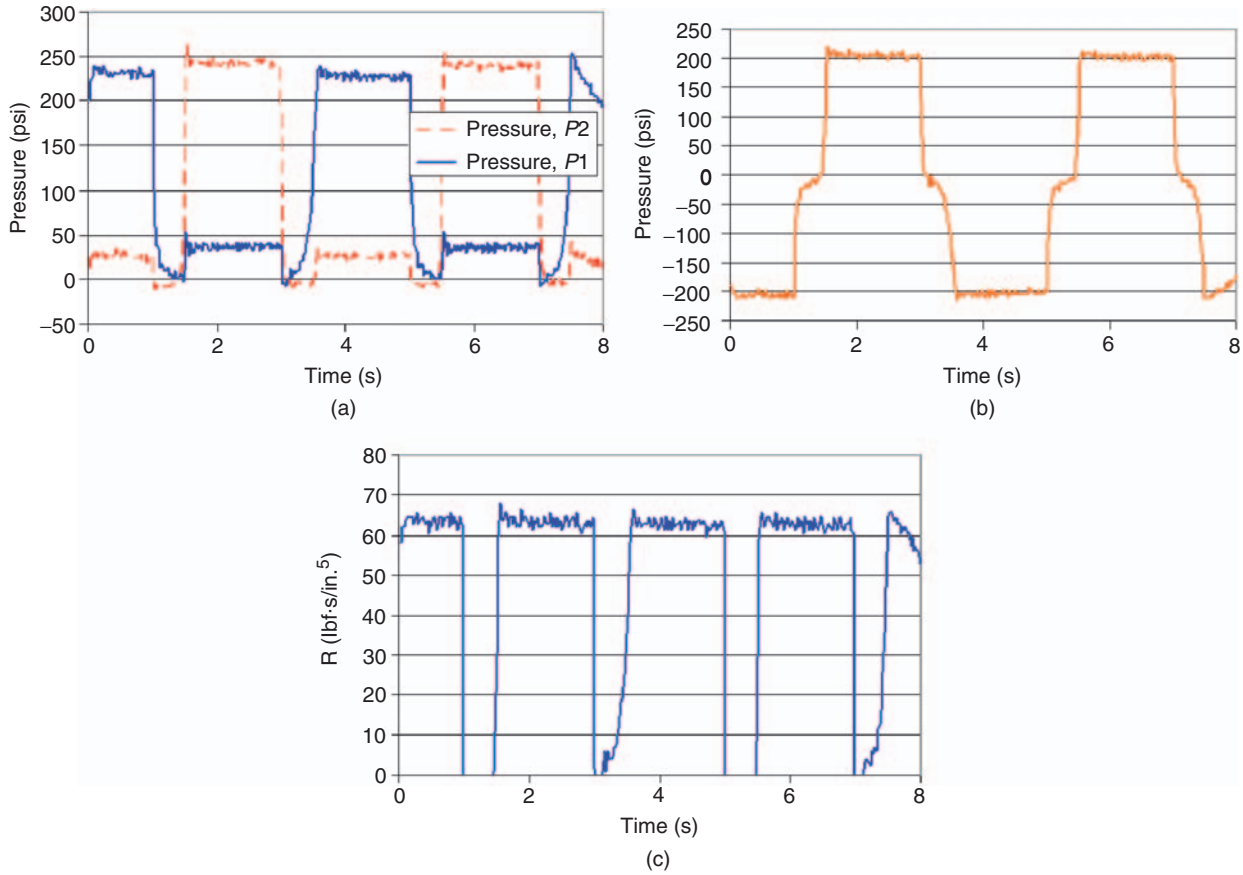

Figure 15. *Left MR fluid valve half measurements for 10 V input, axial gap of 0.125 in. and annular gap of 0.030 in.: (a) Line pressures P1 and P2; (b) pressure differential P2 − P1; and (c) calculated resistance* $R = |P2 - P1|/Q_v$.

The complete set of measurements is summarized in Tables 1 and 2. The valve with annular gap of 0.030 in. achieves greater on-state resistance than the 0.125 in. valve and although its off-state resistance is slightly higher, the overall ratio of on-state to off-state resistance is significantly higher. While this analysis involving only two annular gap values is insufficient to fully characterize the optimal gap for this valve, it is estimated that the optimal value hovers around 0.030 in. This annular gap size is therefore chosen for subsequent valve development.

Table 1. Average resistance measurements for flow directions F1 and F2 in units of lbf s/in.^{5} as a function of input voltage to the valve and axial gap. Coils-in-shaft design; fixed annular gap of 0.030 in.

Voltage (V)	Axial gap (in.)	Resistance F1	Resistance F2
0	0.250	11	12
0	0.125	11	12
0	0.075	12	12
0	0.057	16	17
0	0.036	20	20
5	0.250	49	50
5	0.125	52	53
5	0.075	45	46
5	0.057	72	74
5	0.036	84	91
10	0.250	56	58
10	0.125	60	60
10	0.075	52	53
10	0.057	80	82
10	0.036	93	100

Table 2. Average resistance measurements for flow directions F1 and F2 in units of lbf s/in.^{5} as a function of input voltage to the valve and axial gap. Coils-in-shaft design; fixed annular gap of 0.125 in.

Voltage (V)	Axial gap (in.)	Resistance F1	Resistance F2
0	0.250	9	9
0	0.125	9	9
0	0.075	9	10
5	0.250	16	17
5	0.125	18	18
5	0.075	21	22
10	0.250	19	19
10	0.125	20	21
10	0.075	19	19

MODIFIED VALVE (COILS IN HOUSING)

An additional design objective is to reduce the size of the MR fluid valve both for improving the packaging of the complete system and addressing criterion (iii) outlined in the section 'Actuation results'. To that end, a modified valve design was devised in which the coils were removed from the valve shaft and relocated to the inner housing walls as shown in Figure 16(a) and (b). This permits to reduce the diameter of the conical head piece and connecting valve shaft, while reducing the complexity of the wiring. The magnetic circuit was designed with the assistance of finite element calculations as detailed by Nosse (2005).

From an efficiency point of view, the diameter of the valve shaft must be kept above a minimum value below which magnetic saturation of the shaft occurs. Other factors limiting the miniaturization of the valve include the coil outer diameter, required active MR fluid area,

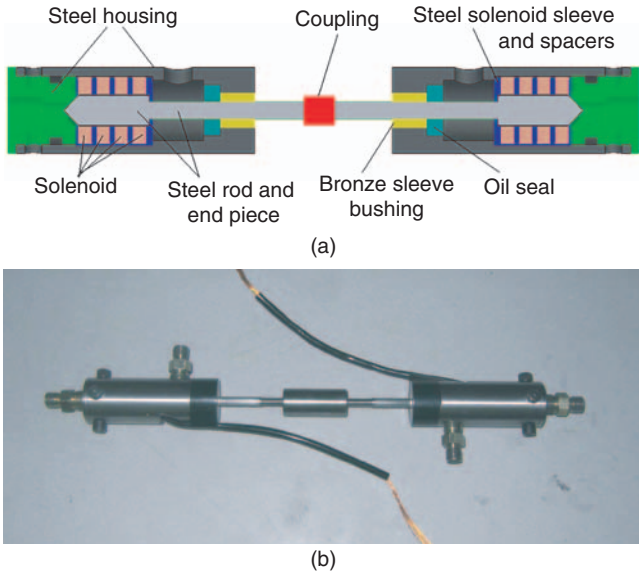

Figure 16. *Redesigned MR fluid valve; (a) cutaway view of a solid model and (b) physical fluid valve. Coil stacks were relocated to the inner housing surface to allow significant size reduction of the movable valve piece.*

type of hydraulic seals, and type of pipe fittings used to connect standard steel fluid lines to the MR valve. These fittings have a tapered thread and require ~0.75 in. below the material surface for machining tool clearance. As shown in Figure 16(a) and (b), the removable housing end-cap was elongated to permit use of these standard fittings. To reduce the size of this removable end-cap, radially oriented bolts were used to fasten the cap to the main housing.

The active MR fluid area is dependent on the placement and size of the coils. Increasing the number of coils within the valve increases not only the activated fluid area, but also the length and electrical impedance of the valve. For this redesign, the number of activated fluid locations was doubled. Finally, the outer diameter dictates the number of wire turns per solenoid. The more turns, the greater the magnetic field produced from an input current. For this redesign, a nominal outside diameter of 1 in. was selected.

In these measurements, the amplitude of the input produced by the universal compression–tension machine was reduced to a value of 2 in. pk–pk to account for the reduced valve volume. To illustrate typical data, in Figure 17(a)–(d) are respectively shown the input flow rate, line pressures, pressure differential, and calculated resistance for a voltage input of 10 V and an axial gap of 0.055 in. The annular gap was fixed in all tests and had a value of 0.030 in. in accordance with the results obtained in the previous section. The pressure differential is respectively positive and negative for flow directions F2 and F1.

The complete set of measurements for the left and right valve halves is respectively summarized in

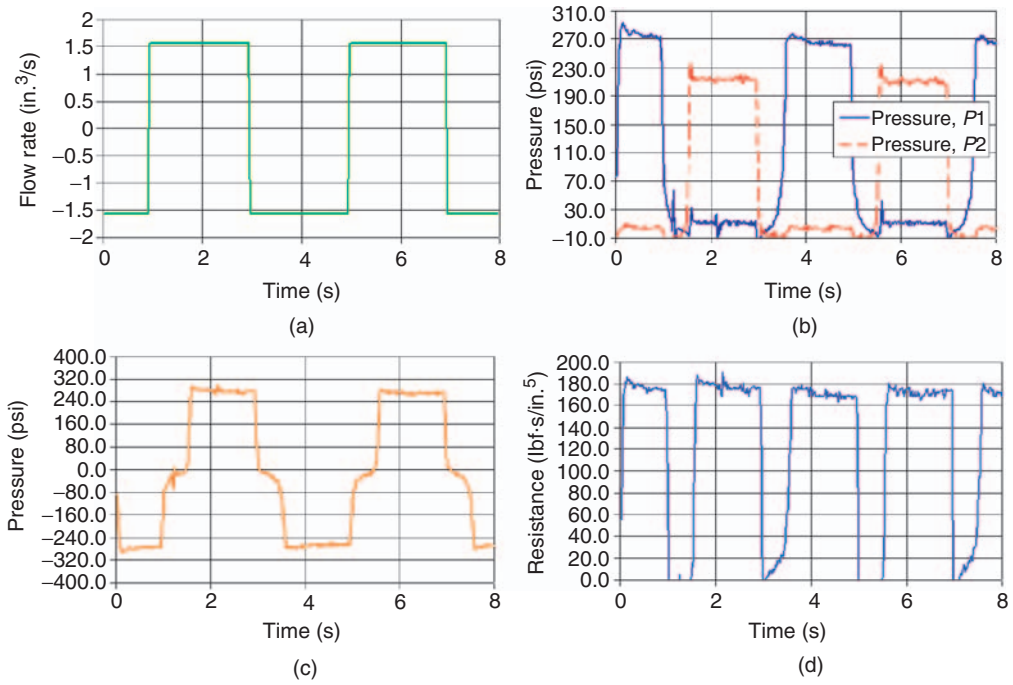

Figure 17. *Redesigned MR valve with solenoids placed in the valve housing, for a 10 V input and 0.055 in. axial gap. The measurements show: (a) input flow rate; (b) line pressures; (c) pressure differential; and (d) calculated resistance* $R = |P2 - P1|/Q_v$.

Table 3. Average resistance measurements in units of lbf s/in.^{5} conducted on the left valve half for fixed annular gap of 0.030 in., as a function of axial gap, solenoid voltage, and flow direction F1 and F2. Coils-in-housing design.

Voltage (V)	Axial gap (in.)	Resistance F1	Resistance F2
0	0.205	10	18
0	0.140	10	19
0	0.055	10	17
3	0.205	73	73
3	0.140	73	73
3	0.055	70	65
6	0.205	52	53
6	0.140	121	127
6	0.055	124	124
10	0.055	172	172

Table 4. Average resistance measurements in units of lbf s/in.^{5} conducted on the right valve half for fixed annular gap of 0.030 in., as a function of axial gap, solenoid voltage, and flow direction F1 and F2. Coils-in-housing design.

Voltage (V)	Axial gap (in.)	Resistance F1	Resistance F2
0	0.205	10	18
0	0.140	10	19
0	0.055	10	17
3	0.205	73	73
3	0.140	73	73
3	0.055	70	65
6	0.205	52	53
6	0.140	121	127
6	0.055	124	124
10	0.055	172	172

Tables 3 and 4. Both halves exhibit a significantly higher on-state resistance than the original design without exhibiting a meaningful increase in off-state resistance. The maximum resistance for the original design is 100 lbf s/in.^{5}, while the redesigned valve has a resistance of 172 lbf s/in.^{5}. This represents a 72% increase in performance over the 570% larger original MR fluid valve. Furthermore, as shown by the constant axial gap plots of the resistance data in Figure 18, the redesigned valve has not yet reached its maximum resistance potential. For the solenoid stacks tested within the valve, voltages higher than 10 V produced significant self-heating. Thus, the input voltage limit was kept below the level at which the MR fluid could fully saturate. The extrapolated curve fit predicts the maximum resistance to occur in the range of 200–250 lbf s/in.^{5} with an input of 20 V.

Similar to the original MR fluid valve, the redesigned valve produces a minimum off-state resistance near 10 lbf s/in.^{5} at all axial gap distances. Therefore, the redesigned valve increases fluid flow resistance by a factor greater than 17 times. The resistance ratio is

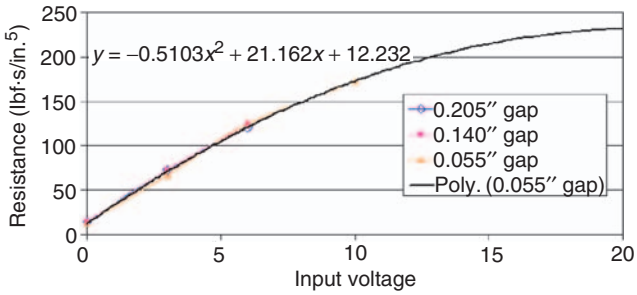

Figure 18. *Projected resistance fit to data for the left half of the redesigned MR fluid valve.*

expected to increase to more than 20 with only minor solenoid modifications.

SYSTEM-LEVEL MODEL

A system-level model for analysis and characterization of the hybrid actuator is presented. The mechanical and fluid regimes are modeled by means of resistance, capacitance, and inductance elements, forming a lumped-parameter system as shown in Figure 19. The MR properties of an MR fluid are characterized by look-up tables based on the measurements described in 'Experiments' section. The controlled inputs applied to the model correspond to the measured quantities saturation voltage applied to the left V_L and right V_R solenoid, acceleration $\ddot{x}$ of the input hydraulic piston, and force F_1 required to accelerate the input piston of mass M.

Application of Newton's second law and force balancing to the input piston yields an expression for the pressure differential produced at the input

$$p_2 - p_1 = \frac{F_1 - M\ddot{x}}{A_{ip}} \tag{2}$$

where A_{ip} denotes the cross-sectional area of the input piston. The volume flow rate is given by

$$Q_{v,net} = \frac{dx}{dt} A_{ip}. \tag{3}$$

Pressure losses occur between the input piston and the valve from flow within the fluid lines. Capacitance is present in the system from MR fluid compressibility and steel line elasticity. These effects are lumped into a common capacitance term C_f located in parallel with the input piston which is dependent upon the pressure differential $p_2 - p_1$. The volume flow rate absorbed by the capacitor is $\tilde{Q}_v$ and the flow rate which travels through the MR fluid valve is Q_v.

$$\tilde{Q}_v = C_f \frac{d(p_2 - p_1)}{dt}, \tag{4}$$

$$Q_v = Q_{v,net} - \tilde{Q}_v. \tag{5}$$

All remaining fluid energy losses occur from resistance and inertia effects. For simplicity, it is assumed that R_1 and I_1 are approximately equal to R_2 and I_2; these variables are set equal to R and I, respectively. The fluid parameters for a circular cross-section fluid lines and parabolic flow are estimated by (Shearer et al., 1997).

$$R = \frac{128\mu L}{\pi d^4}, \tag{6}$$

$$I = 2\left(\frac{\rho}{A}\right)L. \tag{7}$$

The fluid resistance of the output piston $R_{op}(\dot{z})$ is dependent on its travel velocity due to seal friction. The fluid resistance due to static friction is larger than the resistance due to dynamic friction. The variable fluid resistance of the MR fluid valve halves R_L and R_R depends on valve position, magnetic field strength, and flow direction. To address this complex dependency in a phenomenologic manner, the experimental measurements presented in the section 'Fluid resistance measurements' were incorporated into a look-up table. Using interpolated values from the look-up table, the system pressure differentials can be determined,

$$p_4 - p_3 = p_2 - p_1 + 2\left(RQ_v + I\frac{dQ_v}{dt}\right), \tag{8}$$

$$p_4 - p_3 = R_L Q_L + I_L \frac{dQ_L}{dt}, \tag{9}$$

$$p_5 - p_3 = R_R Q_R + I_R \frac{dQ_R}{dt}, \tag{10}$$

$$p_4 - p_5 = R_{op} Q_R, \tag{11}$$

$$p_4 - p_3 = R_R Q_R + I_R \frac{dQ_R}{dt} + R_{op} Q_R. \tag{12}$$

The total flow volume divides into two fluid paths connected in parallel while observing conservation of mass laws

$$Q_v = Q_R + Q_L, \tag{13}$$

$$\frac{dQ_v}{dt} = \frac{dQ_R}{dt} + \frac{dQ_L}{dt}, \tag{14}$$

where Q_R is the volume flow rate of MR fluid through the right valve half and output piston, and Q_L is the volume flow rate through the left valve half. This permits calculation of the volume flow rates through each valve half, as a function of the variable valve-half resistances by setting equations (9) and (12) equal and solving (13) and (14) for Q_R and dQ_R/dt. The resulting flow divider equation has the form

$$(R_R + R_{op} + R_L)Q_R + (I_R + I_L)\frac{dQ_R}{dt} = (R_R + R_{op})Q_v + I_R \frac{dQ_v}{dt}. \tag{15}$$

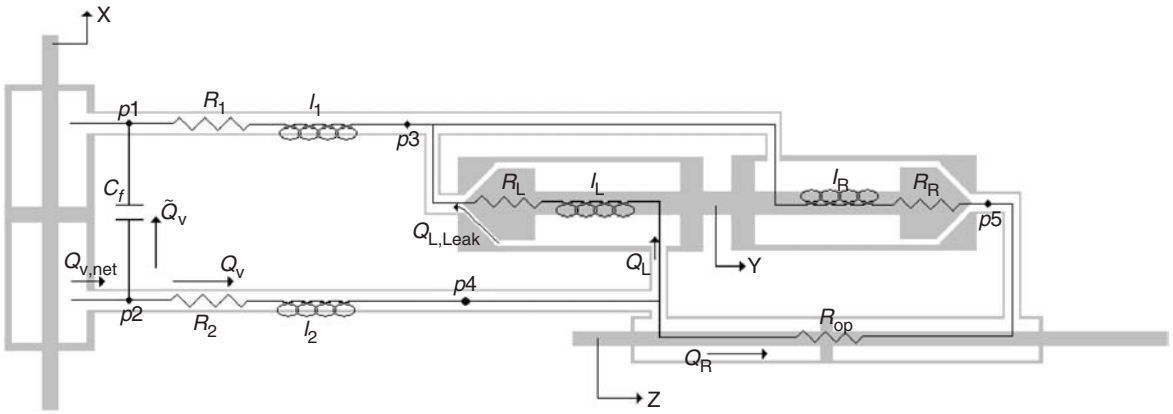

Figure 19. *System-level representation of the hybrid actuator. The fluid flow is represented by resistance, capacitance and inductance elements.*

The fluid leakage across each valve half is a function of the variable valve resistances, which are dependent on valve position y, flow direction, and input voltages V_L and V_R, and the divided volume flow rates. The pertinent experimental measurements shown in section 'Fluid resistance measurements' are also implemented in a look-up table within the simulation to model the leakage output based on resistance and pressure differential inputs. The stored fluid within each valve housing is thus able to control the position y of the fluid valve.

The position of the output piston z and actuation force F_z are modeled by the following equations

$$V_R = \int Q_R, \tag{16}$$

$$z = \frac{V_R}{A_{op}}, \tag{17}$$

$$F_z = \frac{p_4 - p_5}{A_{op}}, \tag{18}$$

where A_{op} is the output piston's cross-sectional area. z is obtained directly from the volume of fluid passing through the right valve half. Solutions to the model equations with parameters obtained from the look-up tables were approximated in SIMULINK.

Model calculations corresponding to the MR valve measurements shown in Figure 7 are shown in Figure 20. The model was cycled between left closed and right closed at a similar frequency of output and an identical amplitude of motion. However, the frequency of the measured valve motion is not exactly constant due to fluctuations in the pressure and flow produced by the manual hydraulic pump. The amplitude of motion in both the model and experiment adhere to the motion limited by rigid constraints at locations within the normalized range of 0–1.

A model simulation of the measurements shown in Figure 11(d) is shown in Figure 21. In this simulation, the voltage input to the left valve half is alternated between on and off in accordance with the physical measurements. As discussed, the right valve half remained off for the entire run. The input acceleration and force are sinusoids and the input solenoid voltage is a square wave. This is similar to the automated experimental inputs produced by the universal compression–tension machine and the LabVIEW control program.

The modeled actuation waveform is a ramped sinusoid, similar to the experimental result shown in Figure 11(d). While the oscillatory shapes are slightly different, both result sets have similar recoil amplitudes of nearly 1 in. pk–pk. While the modeled actuation rate of 0.450 in./s is larger than the experimental result of 0.325 in./s, the discrepancy is not altogether unexpected given the approximate nature of the model. Notwithstanding, the model qualitatively captures the main features of the actuator system.

CONCLUSIONS

This article has presented a new class of hybrid actuator which is based on the rectification of magnetostrictive vibrations by means of MR flow control. The primary focus of the study is to present experiments and theoretical calculations with the goals to substantiate the feasibility of the hybrid actuator and develop design criteria for the development of an effective MR valve. It was established that an MR valve must provide maximum on-state pressure drops while simultaneously exhibiting minimum off-state resistance. While these are stringent demands, the design presented here involving a moving shaft is shown to have the ability to fully close the flow, effectively reaching an infinite pressure drop during part of the on-state cycle. Moreover, the article has presented data which demonstrate the ability of the valve to open and close the flow in a controlled manner in response to electrical input to the valve's solenoids. This has led to actuation measurements which show deflections of 6.5 in. in response to fluid inputs

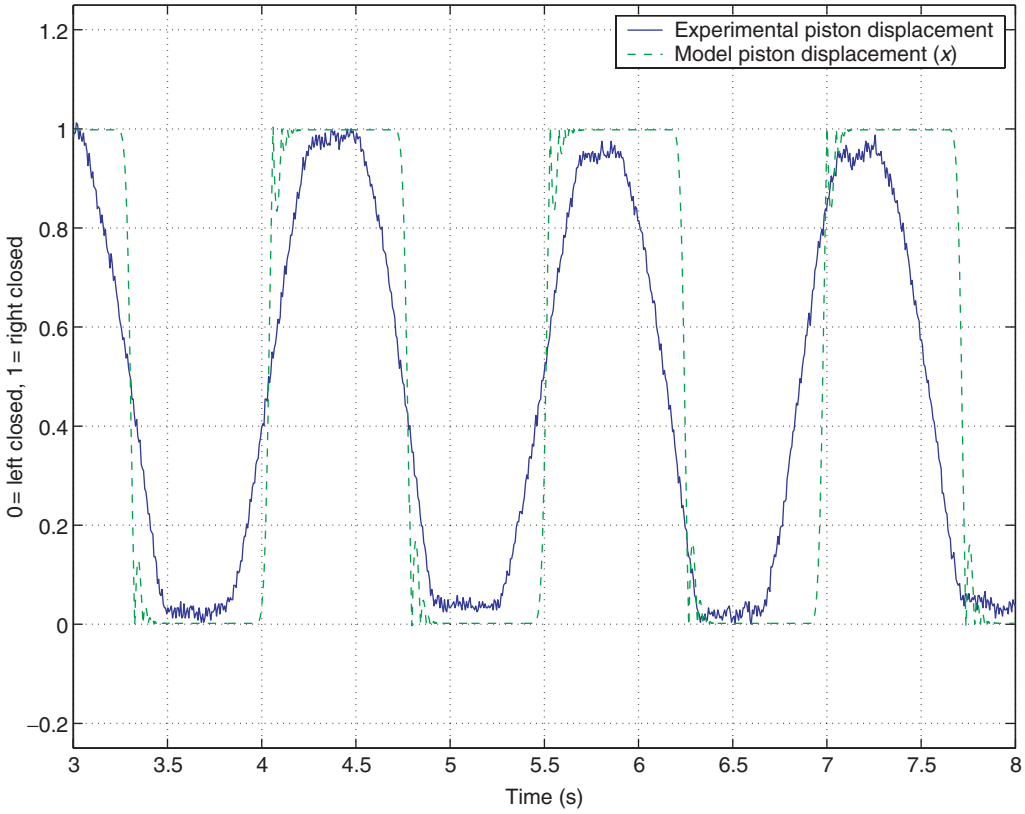

Figure 20. *Comparison between model and the experimental results shown in Figure 7.*

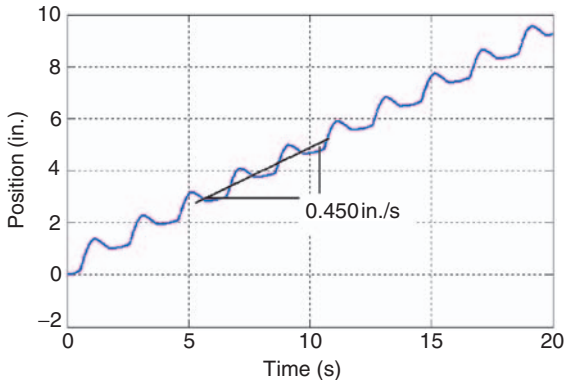

Figure 21. *Model result for the case of controlled actuation shown in Figure 11(d).*

produced with a hydraulic piston in combination with a quasistatic voltage of amplitude 5 V applied to the left valve half. The output deflections are limited only by the size of the output piston. The measurements have also shown significant recoil of the output piston on each cycle of the MR valve. This behavior is attributed to compliances and resistance asymmetries in the fluid network.

A multidomain model of the actuator was developed to better understand the factors that control system behavior and to lay the groundwork for future developments. Improvements to the current model will be focused on improving its fidelity and scope. In particular, the transition profile between left closed and right closed and vice versa is in reality less steep than predicted by the model (Figures 7 and 20). Similarly, the modeled actuation rate of 0.450 in./s is larger than the experimental result of 0.325 in./s (Figures 11(d) and 21). The discrepancies can be attributed to the approximate nature of the systems-level approach employed in the model. The model results and experimental measurements both demonstrate the feasibility of the hybrid actuator presented in this paper.

ACKNOWLEDGMENTS

This work was supported by the Defense Advanced Research Projects Agency (DARPA) (John Main program manager) through Air Force Research Laboratory, Space Vehicle Directorate grant FA9453-03-C-0333 (Benjamin Henderson, Scott Franke and Andrew Williams program monitors). The authors wish to acknowledge William Gillespie and Scott Stacey at Delphi Corporation for supplying the MR fluid used in this investigation.

REFERENCES

Bridger, K., Sewell, J.M., Cooke, A.V., Lutian, J.L., Kohlhafer, D., Small, G.E. and Kuhn, P.M. 2004. "High-pressure Magnetostrictive Pump Development: A Comparison of Prototype and Modeled Performance," In: Anderson, E.H. (ed.), *Proceedings of SPIE Smart Structures and Materials*, Vol. 5388, pp. 246–257, San Diego, CA.

Burton, B., Nosse, D. and Dapino, M.J. 2004. "High Power Density Actuation through Terfenol-D Resonant Motion and Magnetorheological Flow Control," In: *Proceedings of SPIE Smart Structures and Materials*, Vol. 5390, pp. 104–115, San Diego, CA.

Canfield, S. and Frecker, M. 2000. "Topology Optimization of Compliant Mechanical Amplifiers for Piezoelectric Actuators," *Structural and Multidisciplinary Optimization*, 20:269–279.

Choi, Y.Y. and Wereley, N.M. 2004. "Vibration Control of a Landing Gear System Featuring Electrorheological/Magnetorheological Fluids," *Journal of Aircraft*, 40(3):432–439.

Claeyssen, F. and Lhermet, N. 2002. "Actuators based on Giant Magnetostrictive Materials," In: *Proc. Actuator 2002, 8th International Conference on New Actuators*, p. 148, Bremen, Germany.

Cobanoglu, N., Gordaninejad, F., Evrensel, C.A., Liu, Y., Kavlicoglu, B. and Korol, G. 2003. "Time Response of a Controllable Multi-plate Magneto-rheological Fluid Limited Slip Differential Clutch," In: *Proceedings of SPIE Smart Structures and Materials*, Vol. 5056, pp. 514–523, San Diego, CA.

Gerver, M.J., Goldie, J.H., Swenbeck, J.R., Shea, R., Jones, P., Ilmonen, R.T., Dozor, D.M., Armstrong, S., Roderick, R., Nimblett, F.E., Iovanni, R. and Regelbrugge, M.E. 1998. "Magnetostrictive Water Pump," In: *Proceedings of SPIE Smart Structures and Materials*, Vol. 3329, pp. 694–705, San Diego, CA.

Jolly, M.R., Bender, J.W. and Carlson, J.D. 1998. "Properties and Applications of Commercial Magnetorheological Fluids," In: *Proc. SPIE Smart Structures and Materials 1998*, Vol. 3327, pp. 262–275, San Diego, CA.

Jung, H.J., Spencer, B.F., Jr, Ni, Y.Q. and Lee, I.-W. 2004. "State-of-the-art of Semiactive Control Systems using MR Fluid Dampers in Civil Engineering Applications," *Structural Engineering and Mechanics*, 17(3–4):175.

Kiesewetter, L. 1998. "The Application of Terfenol-D in Linear Motors," In: *Proc. 2nd Inter. Conf. Giant Magnetostrictive Alloys*, Marbella, Spain.

Lee, D.G., Wing, S. and Carman, G.P. 2004. "Design of a Piezoelectric-hydraulic Pump with Active Valves," *Journal of Intelligent Material Systems and Structures*, 15:107–115.

Lhermet, N., Claeyssen, F. and Fabbro, H. 2004. "Electro-fluidic Components based on Smart Materials for Aircraft Electro-hydraulic Actuators," In: *Proc. ACTUATOR 2004, 9th Inter. Conf. New Actuators*, Bremen, Germany.

Mauck, L.D. and Lynch, C.S. 2000. "Piezoelectric Hydraulic Pump Development," *Journal of Intelligent Material Systems and Structures*, 11:758–764.

Neelakantan, V.A., Washington, G.N. and Wolf, R. 2002. "Force Feedback System using Magneto-Rheological Fluids for Telerobotic Surgery," In: *Proceedings of SPIE Smart Structures and Materials,* Vol. 4698, pp. 509–518, San Diego, CA.

Nosse, D. 2005. Compact Actuation through Magnetorheological Flow Control and Rectification of Magnetostrictive Vibrations, MSc Thesis, The Ohio State University, Columbus, OH.

Park, J., Carman, G.P. and Hahn, H.T. 2000. "Design and Testing of a Mesoscale Piezoelectric Inchworm Actuator with Microridges," *Journal of Intelligent Material Systems and Structures*, 11:671–684.

Prechtl, E.F. and Hall, S.R. 1999. "Design of High Efficiency, Large Stroke, Electromechanical Actuator," *Smart Materials and Structures*, 8:13–30.

Shearer, J.L., Kulakowski, B.T. and Gardner, J.F. 1997. *Dynamic Modeling and Control of Engineering Systems*, Prentice Hall (2nd Edition).

Sirohi, J. and Chopra, I. 2003. "Design and Development of a High Pumping Frequency Piezoelectric-hydraulic Hybrid Actuator," *Journal of Intelligent Material Systems and Structures*, 14:135–147.

Sirohi, J., Cadou, C. and Chopra, I. 2005. "Investigation of the Dynamic Characteristics of a Piezohydraulic Actuator," *Journal of Intelligent Material Systems and Structures*, 16:481–492.

Teter, J.P., Sendaula, M.H., Vranish, J. and Crawford, E.J. 1998. "Magnetostrictive Linear Motor Development," *IEEE Transactions on Magnetics*, 34:2081–2083.

Yoo, J.-H., Sirohi, J., Wereley, N.M. and Chopra, I. 2003. "A Magnetorheological Hydraulic Actuator Driven by a Piezopump," *Proc. IMECE'03*, Washington, DC.

Yoo, J.-H. and Wereley, N.M. 2004. "Performance of a Magnetorheological Hydraulic Power Actuation System," *Journal of Intelligent Material Systems and Structures*, 15:847–857.

Yoo, J.-H., Sirohi, J. and Wereley, N.M. 2005. "A Magnetorheological Piezo Hydraulic Actuator," *Journal of Intelligent Material Systems and Structures*, 16(11–12):945–954.